Role of Protein Dynamics in Allosteric Control of the Catalytic Phosphoryl Transfer of Insulin Receptor Kinase

Pedro Ojeda-May,[†,§] Yaozong Li,[†,§] Victor Ovchinnikov,[‡,§] and Kwangho Nam[*,†]

[†]Department of Chemistry and Computational Life Science Cluster (CLiC), Umeå University, 901 87 Umeå, Sweden
[‡]Department of Chemistry and Chemical Biology, Harvard University, Cambridge, Massachusetts 02138, United States

S *Supporting Information*

ABSTRACT: The catalytic and allosteric mechanisms of insulin receptor kinase (IRK) are investigated by a combination of ab initio and semiempirical quantum mechanical and molecular mechanical (QM/MM) methods and classical molecular dynamics (MD) simulations. The simulations reveal that the catalytic reaction proceeds in two steps, starting with the transfer of a proton from substrate Tyr to the catalytic Asp1132, followed by the phosphoryl transfer from ATP to substrate Tyr. The enhancement of the catalytic rate of IRK upon phosphorylations in the enzyme's activation loop is found to occur mainly via changes to the free energy landscape of the proton transfer step, favoring the proton transfer in the fully phosphorylated enzyme. In contrast, the effects of the phosphorylations on the phosphoryl transfer are smaller. Equilibrium MD simulations show that IRK phosphorylations affect the protein dynamics of the enzyme before the proton transfer to Asp1132 with only a minor effect after the proton transfer. This finding is consistent with the large change in the proton transfer free energy and the smaller change in the free energy barrier of phosphoryl transfer found by QM/MM simulations. Taken together, the present results provide details on how IRK phosphorylation exerts allosteric control of the catalytic activity via modifications of protein dynamics and free energy landscape of catalytic reaction. The results also highlight the importance of protein dynamics in connecting protein allostery and catalysis to control catalytic activity of enzymes.

Figure 1. (a) Comparison of the active vs inactive conformations of IRK. For the active conformation, the C and N lobes are shown in gray, the activation loop and the DFG motif are shown in blue, the αC helix is shown in yellow, and the substrate peptide is shown in cyan. The substrate Tyr, ATP, the two Mg^{2+} ions, and the three activation-loop phosphotyrosines are shown in ball-and-stick model. For the inactive conformation, only the αC helix (green), the activation loop (red), and the DFG motif are shown for clarity. (b) Proposed Asp1132-assisted catalytic mechanism.

Insulin receptor kinase (IRK) is an important member of protein tyrosine kinase family that catalyzes the transfer of the terminal phosphoryl group of ATP to a Tyr residue of target proteins.[1,2] Like other kinases, IRK is found in two conformations, active and inactive, which differ mainly in the orientations of the activation loop, αC helix, and the Asp-Phe-Gly (DFG) motif (Figure 1a).[2−4] In the inactive conformation (also referred to as the autoinhibited conformation), the activation loop takes an orientation blocking the binding of ATP.[5] Additionally, the αC helix and DFG motif are in their out orientations. In the active conformation, the activation loop swings away from the orientation of the inactive conformation to form a platform for target protein binding and together with the changes of the αC helix and DFG motif orientations opens the active site for ATP binding.[6]

The transition of IRK to its active conformation is triggered by autophosphorylations at three Tyr residues (Tyr1158, 1162, and 1163) in the activation loop. The phosphorylation also increases the enzyme's catalytic activity by about 200-fold relative to that of the unphosphorylated (basally active) IRK. The overall increase is because of (1) increased substrate binding affinities (5−8-fold) and (2) a higher phosphoryl transfer rate (36-fold, corresponding to ∼2.2 kcal/mol lower catalytic barrier) relative to their corresponding unphosphorylated IRK values.[7] Similar results were also reported for insulin-like growth factor 1 receptor kinase (IGF1RK)[8] and protein kinase A.[9] Although the crystal structures of IRK[5,6] in the active and inactive conformations may provide insights into the increased substrate binding affinities, it remains unclear how the phosphoryl groups in the activation loop, which are remote from both the ATP and the Tyr of target protein, exert effects on the catalytic rate (i.e, k_{cat}) of IRK.

To understand the role of the activation loop phosphorylations at the molecular level, we calculate profiles of the reaction free energy using two independent methods, umbrella sampling (US)[10] and the string method (SM).[11] In the simulations, we apply the recently developed multiscale ab initio (AI)[12] and semiempirical QM/MM methods[13,14] to model the catalytic reaction. All simulations are carried out on

the basis of the X-ray crystal structure of the active conformation IRK (Protein Database ID: 1IR3)[6] with a fully phosphorylated activation loop, ATP, and substrate peptide and the assumption that this conformation is the catalytically competent one. Simulation details are provided in Supporting Information. In the study, we focus on the catalytic mechanism, in which the catalytic Asp1132 acts as the general base, abstracting a proton from the Tyr of the substrate peptide (Figure 1b).[6,15] Asp1132 is well-positioned for the proposed proton abstraction from the substrate Tyr in the active conformation of IRK,[6] and a similar catalytic mechanism has been suggested in other protein kinases.[16−19] Figure S1 shows that this mechanism is favored in IRK versus other mechanisms, such as the substrate-assisted mechanism, in which one of the transferring phosphoryl oxygens acts as the general base. Figure S1 also shows that catalysis occurs in a stepwise manner with the proton transfer to Asp1132 taking place in advance of the nucleophilic attack at the terminal phosphorus of ATP by the substrate Tyr. Below, we examine each reaction step in detail and discuss the implications to catalysis.

First, the phosphoryl transfer step is examined by the US[10] free energy (US-FE) simulations. For sufficient sampling of the enzyme and water configurations, the semiempirical AM1/d-PhoT QM/MM potential[13] is used in the simulation with the simple valence-bond-like (SVB) corrections[14] applied to the bonds involved in the phosphoryl transfer reaction, i.e., cleaving $O_{\beta\gamma}-P_{\gamma}$ and forming $P_{\gamma}-O_{Tyr}$ bonds (hereafter, the AM1/d-SVB method). The results are presented in Figure 2b. For the
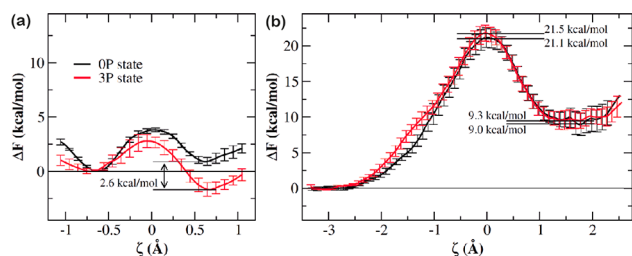
Figure 2. Free energy profiles for (a) the proton transfer and (b) the phosphoryl transfer steps, determined from umbrella sampling simulations: 3P refers the fully phosphorylated IRK, and 0P refers to the unphosphorylated IRK. The reaction coordinate, ζ, is defined as (a) the distance difference between the $O_{Tyr}-H_{Tyr}$ and $H_{Tyr}-O_{\delta Asp}$ bonds and (b) that between the $O_{\beta\gamma}-P_{\gamma}$ and $P_{\gamma}-O_{Tyr}$ bonds.

fully phosphorylated IRK, the AM1/d-SVB QM/MM result is also compared in Figure S2a to the results of the multiscale AI-QM/MM simulations (i.e., the AI-QM/MM results). In the AI-QM/MM simulation, the B3LYP[20,21] density functional theory is used as the ab initio QM theory. The comparison shows that the AM1/d-SVB QM/MM method overestimates the barrier height only by 4.3 kcal/mol (17.2 kcal/mol for the AI-QM/MM method vs 21.5 kcal/mol for the AM1/d-SVB QM/MM method) and yields a reaction free energy very close to the value of the AI-QM/MM result (9.0 kcal/mol for the AI-QM/MM method vs 9.3 kcal/mol for the AM1/d-SVB QM/MM method). On the basis of the result, we thus use the 4.3 kcal/mol value as a correction factor of the phosphoryl transfer barrier determined at the AM1/d-SVB QM/MM level of theory.

For each set of coordinates saved during the US-FE (AM1/d-SVB QM/MM) simulations, bond orders of the forming and cleaving P−O bonds are determined using the approach of

Armstrong et al.[22] The results are presented in Figure S2b for the fully phosphorylated IRK. Around the transition state (TS), the two P−O bonds exhibit very similar bond orders (~0.2; Figure S3) and bond lengths (2.2 ± 0.1 Å for the cleaving P−O bond and 2.2 ± 0.2 Å for the forming P−O bond), suggesting that the reaction occurs by a concerted mechanism between the two P−O bonds with a slightly loose dissociative TS. (The mechanism is considered associative if the forming P−O bond distance at TS < 1.9 Å and loose dissociative with the P−O bond distance around 2.5 Å or longer.)[15,23] The significance of a loose TS with a relatively flat TS free energy surface in enzyme catalysis has been discussed previously.[24,25] The present result differs from that of Zhou and Wong,[15] who employed a potential energy scan to study IRK catalysis. They found that the reaction occurs by an asynchronous concerted mechanism between the proton and the phosphoryl transfer steps, and that the TS P−O bonds are longer (2.41 Å for the cleaving and 2.32 Å for the forming P−O bond) than the present values. We attribute the difference of the results to the difference of the approaches used in the two works. Zhou and Wong considered only the potential energy scan, which ignores the effects of environmental relaxation on the reaction. By contrast, our approach considers the change of free energies via explicit sampling of protein and water configurations from a thermodynamic ensemble. This allows full relaxation of the environment during the reaction and thus is more physically realistic.[26,27]

To examine the effects of the activation loop phosphorylations on the phosphoryl transfer step, US-FE (AM1/d-SVB QM/MM) simulations are also carried out for the unphosphorylated IRK. The results show that the phosphoryl transfer barrier and the reaction free energy of the unphosphorylated IRK are very similar to their corresponding values in the fully phosphorylated IRK (Figure 2b). The barrier height and the reaction free energy of the unphosphorylated IRK are 21.1 kcal/mol (16.8 kcal/mol after the 4.3 kcal/mol AI-QM/MM correction) and 9.0 kcal/mol (Table S1), respectively. The close similarity between the two FE profiles suggests that the phosphoryl transfer step is not affected strongly by the phosphoryl groups in the activation loop. The result implies that the phosphorylations must induce changes in the proton transfer step to yield the experimentally observed increase of the catalytic rate in the fully phosphorylated IRK.[7] Indeed, we find that the free energy of the proton transfer reaction is lower by 2.6 kcal/mol in the fully phosphorylated IRK than the value in unphosphorylated IRK (Figure 2a).

How much does the difference in the proton transfer free energy affect the overall catalytic barrier? To address the question, we use the string method free energy (SM-FE) simulations[11] to compute the free energy profile along the entire combined proton and phosphoryl transfer reaction path. (See Supporting Information for details.) The FE profiles, presented in Figure 3, show that the proton transfer free energy in the fully phosphorylated IRK is lower by 2.5 kcal/mol than that in the unphosphorylated IRK. In addition, the effects of the activation loop phosphorylations on the phosphoryl transfer barrier is found to be relatively small (21.1 kcal/mol in the fully phosphorylated IRK vs 22.1 kcal/mol in the unphosphorylated IRK), consistent with the US-FE simulations. Relative to the lowest free energy state of each IRK, the overall catalytic barrier is 22.5 kcal/mol in the fully phosphorylated IRK and 24.5 kcal/mol in the unphosphorylated IRK (Table S1). After the AI-QM/MM correction, they are 18.2 and 20.2 kcal/mol,
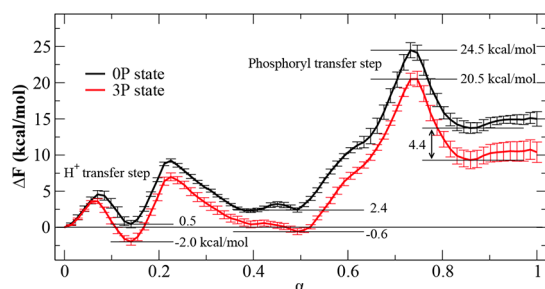
Figure 3. Free energy profile along the entire proton and phosphoryl transfer reaction path determined from the string method simulations. The path is described by a parametrized progress variable, α, which varies between 0.0 for the state before the proton transfer and 1.0 after the phosphoryl transfer step. The notation and color of each profile are the same as those in Figure 2.

respectively, which agree well with the experimental estimates of 15.4 kcal/mol for the fully active IRK and 17.6 kcal/mol for the basally active IRK.[7] More importantly, the difference between the two barriers agrees quantitatively between the computation and experiments (2.0 kcal/mol from the present simulation and 2.2 kcal/mol from experiments[7]). Very similar results are also deduced from the composite US-FE profiles (Figure S3).

The present QM/MM simulations show that the rate enhancement in the fully phosphorylated IRK is achieved early in the reaction via modifications to the reaction free energy of the proton transfer step to favor the proton transfer reaction product in the fully phosphorylated IRK. This then shifts the phosphoryl transfer free energy surface to lower the overall catalytic barrier. Unexpectedly, the IRK phosphorylation exerts a smaller effect on the (intrinsic) phosphoryl transfer barrier. Because the phosphoryl transfer is the core catalytic function of all kinases, one would expect this step to be the main catalytic step under allosteric control. To gain insight into how the IRK phosphorylation affects the free energy of proton transfer to Asp1132 and to a lesser extent the phosphoryl transfer step, we have carried out classical MD simulations. (See Supporting Information for details.)

To illustrate the differences in the dynamics of IRK in three states (i.e., inactive, active prior to the proton transfer, and active after proton transfer), we show covariance matrices of atomic fluctuations in Figure 4. The figure makes clear that

phosphorylations in the activation loop increase correlated protein motions in IRK before the proton transfer to Asp1132. The most obvious increase is observed in the fully phosphorylated active conformation IRK (Figure 4b). In this system, the cross-correlation is increased substantially throughout the entire protein, which suggests that conformational fluctuations are substantially diminished, i.e., the enzyme becomes more rigid when its activation loop is phosphorylated. A similar but slightly smaller increase of the cross-correlation is also observed in the inactive conformation after the activation loop phosphorylations (Figure 4a). The decreased conformational fluctuation upon IRK phosphorylation is consistent with earlier prediction by Bishop et al.[28] On the basis of unfolding experiments, they reported that IRK loses some of its conformational free energy upon the activation loop phosphorylations. In contrast, we find that after the proton transfer, the two covariance matrices corresponding to the fully phosphorylated and unphosphorylated IRKs show only small differences (Figure 4c). This implies not only that the dynamics of the fully phosphorylated IRK change again after the proton transfer, but also that the change occurs in a direction to reverse the effects of activation loop phosphorylations, yielding protein dynamics similar to those of the unphosphorylated IRK.

Notably, the MD simulation results are consistent with the results of the QM/MM simulations. For instance, the decrease of cross-correlations in the fully phosphorylated IRK after the proton transfer (compare Figures 4b,c) suggests that the conformational entropy of IRK increases during or after the proton transfer. Because the enzyme is allowed to move freely during the free energy simulations, an increase in the conformational entropy of the enzyme would be reflected in the lower free energy of proton transfer in the fully phosphorylated IRK, as observed in Figures 2a and 3. In addition, the fact that the phosphoryl transfer barriers are affected by phosphorylations to a lesser extent than the proton free energies (Figures 2b and 3) is consistent with the relatively unchanged cross-correlation maps shown in Figure 4c. We have also examined a potential effect of the activation loop phosphoryl groups on the barrier height using the energy decomposition analysis. The results shown in Figure S4 suggest that electrostatic interactions involving the phosphoryl groups affect to some extent the proton transfer but not the phosphoryl transfer step.
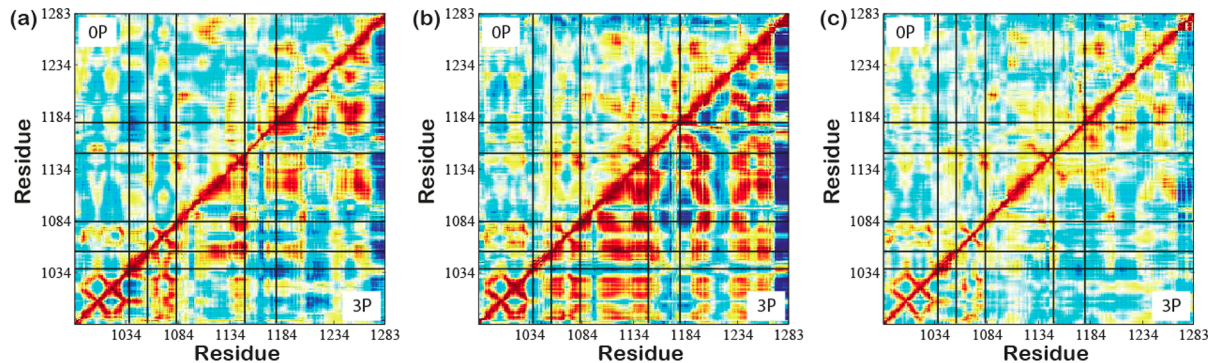
Figure 4. Covariance map of atomic fluctuations of IRK: (a) inactive conformation, (b) active conformation before the proton transfer, and (c) active conformation after completing the proton transfer. For each figure, the covariance map of the unphosphorylated IRK (0P) is shown in the upper-left triangle and that of the fully phosphorylated IRK (3P) is shown in the lower-right triangle. The color scale changes from blue (−0.6 or below) for anticorrelated atomic motions to white (zero) for uncorrelated motions and to red (0.6 and higher) for correlated motions between a pair of amino acid residues.

Here, we have examined the catalytic mechanism of insulin receptor kinase (IRK) and the role of the enzyme's activation loop phosphorylations in catalysis using multiscale ab initio and semiempirical QM/MM methods as well as classical MD simulations. IRK catalyzes the reaction in two steps: the transfer of substrate Tyr proton to Asp1132, followed by the phosphoryl transfer to Tyr. The enhancement of the catalytic rate by IRK phosphorylation is achieved by lowering the proton transfer reaction free energy without major change of the intrinsic phosphoryl transfer barrier. MD simulations show that protein dynamics of IRK are affected substantially by the activation loop phosphorylations. However, after the proton transfer, they become very similar to the protein dynamics of the basally active IRK. Taken together, the present results suggest that allosteric control of the catalytic activity of IRK is achieved via a modification of the catalytic reaction free energy landscape, in which protein dynamics and electrostatic interactions play crucial roles. The importance of protein dynamics in allostery has also been suggested in other systems.[29−34] Follow up studies, such as detailed characterization of protein dynamics in different metastable states identified from the present work and conformational transition between them will further increase our understanding of the roles of the activation loop phosphorylations in controlling the catalytic activity of this important kinase.

◼ ASSOCIATED CONTENT

Ⓢ Supporting Information

The Supporting Information is available free of charge on the ACS Publications website at DOI: 10.1021/jacs.5b07996.

Computational details and supporting tables and figures. (PDF)

◼ AUTHOR INFORMATION

Corresponding Author

*kwangho.nam@chem.umu.se

Author Contributions

§These authors contributed equally.

Notes

The authors declare no competing financial interest.

◼ ACKNOWLEDGMENTS

◼ REFERENCES

(1) van der Geer, P.; Hunter, T.; Lindberg, R. A. *Annu. Rev. Cell Biol.* **1994**, *10*, 251−337.

(2) Endicott, J. A.; Noble, M. E. M.; Johnson, L. N. *Annu. Rev. Biochem.* **2012**, *81*, 587−613.

(3) Hubbard, S. R.; Till, J. H. *Annu. Rev. Biochem.* **2000**, *69*, 373−398.

(4) Nolen, B.; Taylor, S.; Ghosh, G. *Mol. Cell* **2004**, *15*, 661−675.

(5) Hubbard, S. R.; Wei, L.; Ellis, L.; Hendrickson, W. A. *Nature* **1994**, *372*, 746−754.

(6) Hubbard, S. R. *EMBO J.* **1997**, *16*, 5572−5581.

(7) Ablooglu, A. J.; Kohanski, R. A. *Biochemistry* **2001**, *40*, 504−513.

(8) Favelyukis, S.; Till, J. H.; Hubbard, S. R.; Miller, W. T. *Nat. Struct. Biol.* **2001**, *8*, 1058−1063.

(9) Steichen, J. M.; Kuchinskas, M.; Keshwani, M. M.; Yang, J.; Adams, J. A.; Taylor, S. S. *J. Biol. Chem.* **2012**, *287*, 14672−14680.

(10) Torrie, G. M.; Valleau, J. P. *J. Comput. Phys.* **1977**, *23*, 187−199.

(11) Ovchinnikov, V.; Karplus, M.; Vanden-Eijnden, E. *J. Chem. Phys.* **2011**, *134*, 085103.

(12) Nam, K. *J. Chem. Theory Comput.* **2014**, *10*, 4175−4183.

(13) Nam, K.; Cui, Q.; Gao, J.; York, D. M. *J. Chem. Theory Comput.* **2007**, *3*, 486−504.

(14) Devi-Kesavan, L. S.; Garcia-Viloca, M.; Gao, J. *Theor. Chem. Acc.* **2003**, *109*, 133−139.

(15) Zhou, B.; Wong, C. F. *J. Phys. Chem. A* **2009**, *113*, 5144−5150.

(16) Adams, J. A. *Chem. Rev.* **2001**, *101*, 2271−2290.

(17) Valiev, M.; Kawai, R.; Adams, J. A.; Weare, J. H. *J. Am. Chem. Soc.* **2003**, *125*, 9926−9927.

(18) Cheng, Y.; Zhang, Y.; McCammon, J. A. *J. Am. Chem. Soc.* **2005**, *127*, 1553−1562.

(19) Smith, G. K.; Ke, Z.; Guo, H.; Hengge, A. C. *J. Phys. Chem. B* **2011**, *115*, 13713−13722.

(20) Becke, A. D. *J. Chem. Phys.* **1993**, *98*, 5648−5652.

(21) Lee, C.; Yang, W.; Parr, R. G. *Phys. Rev. B: Condens. Matter Mater. Phys.* **1988**, *37*, 785−789.

(22) Armstrong, D. R.; Perkins, P. G.; Stewart, J. J. P. *J. Chem. Soc., Dalton Trans.* **1973**, 838−840.

(23) Mildvan, A. S. *Proteins: Struct., Funct., Genet.* **1997**, *29*, 401−416.

(24) Ma, B.; Kumar, S.; Tsai, C.-J.; Hu, Z.; Nussinov, R. *J. Theor. Biol.* **2000**, *203*, 383−397.

(25) Ma, B.; Nussinov, R. *Curr. Opin. Chem. Biol.* **2010**, *14*, 652−659.

(26) Gao, J.; Ma, S.; Major, D. T.; Nam, K.; Pu, J.; Truhlar, D. G. *Chem. Rev.* **2006**, *106*, 3188−3209.

(27) Masgrau, L.; Truhlar, D. G. *Acc. Chem. Res.* **2015**, *48*, 431−438.

(28) Bishop, S. M.; Ross, J. B. A.; Kohanski, R. A. *Biochemistry* **1999**, *38*, 3079−3089.

(29) Young, M. A.; Gonfloni, S.; Superti-Furga, G.; Roux, B.; Kuriyan, J. *Cell* **2001**, *105*, 115−126.

(30) Cheng, Y.; Zhang, Y.; McCammon, J. A. *Protein Sci.* **2006**, *15*, 672−683.

(31) Masterson, L. R.; Shi, L.; Metcalfe, E.; Gao, J.; Taylor, S. S.; Veglia, G. *Proc. Natl. Acad. Sci. U. S. A.* **2011**, *108*, 6969−6974.

(32) Nam, K.; Pu, J.; Karplus, M. *Proc. Natl. Acad. Sci. U. S. A.* **2014**, *111*, 17851−17856.

(33) Vanatta, D. K.; Shukla, D.; Lawrenz, M.; Pande, V. S. *Nat. Commun.* **2015**, *6*, 7283.

(34) Malmstrom, R. D.; Kornev, A. P.; Taylor, S. S.; Amaro, R. E. *Nat. Commun.* **2015**, *6*, 7588.